Available online at www.sciencedirect.com
SCIENCE DIRECT®
International Journal of Heat and Mass Transfer 47 (2004) 1335–1346
International Journal of HEAT and MASS TRANSFER
www.elsevier.com/locate/ijhmt

Numerical simulation of forced convective evaporation system for tannery effluent

G.V.S. Sesha Girish, A. Mani *

Department of Mechanical Engineering, Refrigeration and Airconditioning Laboratory, Indian Institute of Technology Madras, Chennai 600 036, India

Received 4 February 2003; received in revised form 8 August 2003

Abstract

A numerical technique for evaluating the performance of forced convective evaporation system for tannery effluent is presented. The paper describes a mathematical model, which treats the airflow to be two dimensional and liquid flow to be one-dimensional. The turbulence in airflow is modeled with low Reynolds number k–ε model. The interface heat and mass transfer are represented by Reynolds flux model. The governing equations are solved using a modified MAC (Marker and Cell) method. The model is embodied into a computer code, which is applicable to forced convective evaporation system as well as mechanical draft cooling towers of both counter flow and cross flow types. Predicted results compare well with the available data in the literature and with that of experimental data and give closer results than the existing models. Distributions of air velocities, pressure, moisture fraction and air and water temperatures have been presented. The model can be used as design as well as optimization tool.

Keywords: Forced convective evaporation; Tannery effluent; Numerical simulation; MAC method; k–ε model

1. Introduction

Tannery effluent (soak liquor) is one of the liquid wastes produced in leather tanning industry. It consists 2–3% sodium chloride salt. If let out without treatment, the soak liquor causes severe pollution. One of the ways to contain this is by evaporating the water in the liquor and recovering the salt. Forced convective evaporation system is one among such systems [7]. The system is essentially of cooling tower type, with the main objective being to evaporate the liquor. Soak liquor is sprayed in an enclosed tower and air is drawn up against the falling liquor. Packing material is used to increase the contact area and residence time. Heat and mass transfer occur between liquor and air and some of the liquor gets evaporated. The schematic diagram of the system is shown in Fig. 1.

The first attempt at modeling the transfer processes taking place in evaporative cooling tower was made by Merkel [5] in 1926. With many assumptions he combined the heat and mass transfer processes and introduced the enthalpy driving potential concept. Merkel's method has been in use for decades. Baker and Shryock [4] examined the effects of approximations in Merkel's method and suggested means of reducing some of the errors. Sutherland [9] did accurate analysis by considering the mass of water evaporated. Marseille et al. [11] described a one-dimensional model by accounting the liquid-side film resistance.

The methods described earlier for designing a cooling tower and solving the governing equations often assume uniformity of upward air flow and downward liquid flow. But the flow of air and water inside the tower can exhibit large variations because of the tower

* Corresponding author. Tel.: +91-44-2257-8534; fax: +91-44-2257-0509.
E-mail address: mania@iitm.ac.in (A. Mani).

0017-9310/$ - see front matter
doi:10.1016/j.ijheatmasstransfer.2003.10.001

Nomenclature

f	resistance to air flow
g	acceleration due to gravity, m s^{-2}
G	mass flow rate of air, kg s^{-1}
h	specific enthalpy, kJ kg^{-1}
k	turbulent kinetic energy, m^2 s^{-2}
L	mass flow rate of liquor, kg s^{-1}
L_c	characteristic length, m
M	molecular weight, g mol^{-1}
p	pressure, bar
R	radius, m
Re	Reynolds number
Pr	Prandtl number
t	time, s
T	temperature, K
u	velocity in x direction, m s^{-1}
v	velocity in r direction, m s^{-1}
x, r	coordinates, m

Greek symbols

α	thermal diffusivity, m^2 s^{-1}
v	kinematic viscosity, m^2 s^{-1}
ρ	density, m^3 kg^{-1}

Subscripts

a	air
i	interface
l	liquor
t	turbulent
m	mean

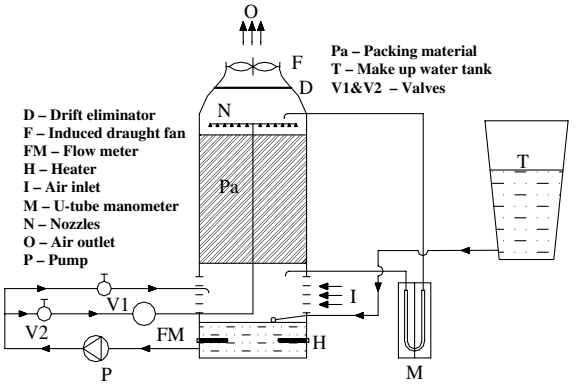

Fig. 1. Schematic diagram of forced convective evaporation system.

geometry, packing material, fan, variable liquid loading and interactions between air and liquid. Majumdar et al. [2] discussed the limitations of one-dimensional models and described a better model. Local heat and mass transfer rates were calculated with empirical coefficients. Current literature shows there is no generally accepted method exists for predicting the performance of a cooling tower.

In order to predict the thermal performance of a system, an accurate mathematical model is needed to solve the governing equations. Physical models are also needed to represent the flow and interface heat and mass transfer processes accurately. This study is aimed at improving existing models and meets the above said requirements with a new mathematical model for predicting the thermal performance of the forced convective evaporation system. The modified MAC (Marker and Cell) method is used for solving the governing equations.

2. Mathematical model

In mechanical draft systems, air changes its direction as it enters the tower horizontally and leaves vertically. This non-uniformity in airflow distribution can be accounted for only by performing two- or three-dimensional analysis. The flow is essentially turbulent because of the geometry, packing material, fan and liquid–air interaction. The liquid flow is predominantly downward and hence can be assumed to be one-dimensional. The present model treats the airflow in the system to be two-dimensional, axisymmetric and turbulent. Governing equations for air include conservation equations for mass continuity, momentum, energy and mass fraction of moist air. Liquor flow is governed by mass continuity and energy equations.

The computational domain extends from the vertical inlet plane to the horizontal outlet section as shown in Fig. 2. As the problem is axisymmetric, only half of the domain is considered. The non-dimensional governing equations are

Mass continuity of air:

$$\frac{\partial}{\partial x^*}(u^*) + \frac{1}{r^*}\frac{\partial}{\partial r^*}(r^* v^*) = m'''^* \tag{1}$$

x-direction momentum of air:

$$\frac{\partial}{\partial x^*}(u^{*2}) + \frac{1}{r^*}\frac{\partial}{\partial r^*}(r^* u^* v^*) = -\frac{1}{\rho^*}\frac{\partial p^*}{\partial x^*} - f_x^* + \frac{\partial}{\partial x^*}\left\{\frac{1}{Re}(1+Re_t)\frac{\partial u^*}{\partial x^*}\right\} + \frac{1}{r^*}\frac{\partial}{\partial r^*}\left\{r^*\frac{1}{Re}(1+Re_t)\frac{\partial u^*}{\partial r^*}\right\} - g^* \tag{2}$$

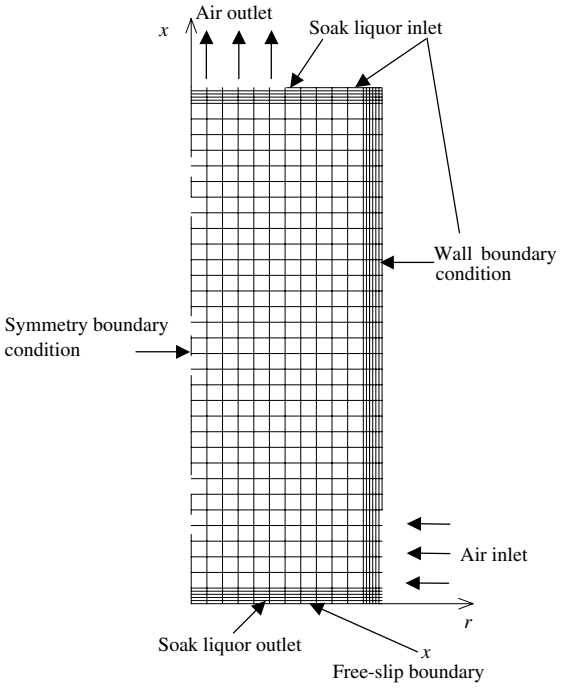

Fig. 2. Computational domain and grid.

r-direction momentum of air:

$$\frac{\partial}{\partial x^*}(u^*v^*) + \frac{1}{r^*}\frac{\partial}{\partial r^*}(r^*v^{*2}) = -\frac{1}{\rho^*}\frac{\partial p^*}{\partial r^*} - f_r^* + \frac{\partial}{\partial x^*}\left\{\frac{1}{Re}(1+Re_t)\frac{\partial v^*}{\partial x^*}\right\} + \frac{1}{r^*}\frac{\partial}{\partial r^*}\left\{r^*\frac{1}{Re}(1+Re_t)\frac{\partial v^*}{\partial r^*}\right\} \quad (3)$$

Energy equation of air:

$$\frac{\partial}{\partial x^*}(u^*T_a^*) + \frac{1}{r^*}\frac{\partial}{\partial r^*}(r^*v^*T_a^*) = \frac{\partial}{\partial x^*}\left\{\frac{1}{Re}(1+Re_tPr_t)\frac{\partial T_a^*}{\partial x^*}\right\} + \frac{1}{r^*}\frac{\partial}{\partial r^*}\left\{r^*\frac{1}{Re}(1+Re_tPr_t)\frac{\partial T_a^*}{\partial r^*}\right\} + q'''^* \quad (4)$$

Moisture fraction of air:

$$\frac{\partial}{\partial x^*}(u^*f_a^*) + \frac{1}{r^*}\frac{\partial}{\partial r^*}(r^*v^*f_a^*) = \frac{\partial}{\partial x^*}\left(\frac{1}{Re}(1+Re_tPr_t)\frac{\partial f_a^*}{\partial x^*}\right) + \frac{1}{r^*}\frac{\partial}{\partial r^*}\left(r^*\frac{1}{Re}(1+Re_tPr_t)\frac{\partial f_a^*}{\partial r^*}\right) + m'''^* \quad (5)$$

Mass continuity of liquor:

$$\frac{\partial}{\partial x^*}(\rho_l^*u_l^*) = -m'''^* \quad (6)$$

Energy equation for liquor:

$$\frac{\partial}{\partial x}(\rho_l^*c_lu_l^*T_l^*) = -q'''^* \quad (7)$$

The non-dimensional parameters used are

$$u^* = \frac{u}{U}, \quad v^* = \frac{v}{U}, \quad u_l^* = \frac{u_l}{U}, \quad x^* = \frac{x}{R_r}, \quad r^* = \frac{r}{R_r}, \quad \rho^* = \frac{\rho_a}{\rho_\infty}, \quad \rho_l^* = \frac{\rho_l}{\rho_\infty} \quad (8)$$

$$p^* = \frac{p}{\rho_\infty U_\infty^2}, \quad f_x^* = \frac{f_x}{(U_\infty^2/R_r)}, \quad f_r^* = \frac{f_r}{(U_\infty^2/R_r)}, \quad g^* = \frac{g}{(U_\infty^2/R_r)} \quad (9)$$

$$T_a^* = \frac{T-T_\infty}{T_{lo}-T_\infty}, \quad T_l^* = \frac{T-T_{lo}}{T_{li}-T_{lo}}, \quad \alpha^* = \frac{\alpha}{\alpha_\infty}, \quad v^* = \frac{v}{v_\infty} \quad (10)$$

$$m'''^* = \frac{m'''}{(\rho_\infty U/R_r)}, \quad q'''^* = \frac{q'''}{(\rho_\infty U(T_{li}-T_\infty)/R_r)} \quad (11)$$

where U is the reference velocity, taken equal to inlet velocity; R_r is the reference length, taken equal to radius of tower; subscript ∞ refers to free stream conditions, i.e., air at inlet.

Conservation equations for air are coupled through convective terms (ρu and ρv) and momentum equations are coupled through pressure. m''' and q''' represent the source terms for mass and heat transfer respectively. f_x and f_r represent the resistances to airflow in the axial and radial directions respectively due to the presence of solid objects.

3. Physical models

3.1. Turbulence

The solution of the problem of turbulent flow can be obtained by direct numerical simulation (DNS) of the time dependent Navier–Stokes equations. However, this approach is very expensive in terms of memory and computational resources and time. Another approach is to take time average of the governing equations and solve them. Since the solution of the time-averaged equations is preferred approach for engineering calculations, turbulence models gained importance. Among all two equations turbulence models, k–ε model is versatile because of its range of applicability less computational effort. Jones and Launder [12] were first to propose a k–ε model, which is valid for both low and high Reynolds numbers. The low Reynolds number k–ε turbulence model of Jones and launder is used in the present model. This model avoids the use of wall functions in the viscosity affected near wall region. Flow is

represented by time-averaged equations. The model equations for k and ε in non-dimensional form are

$$\begin{aligned}&\frac{\partial}{\partial x^*}(u^*k^*)+\frac{1}{r^*}\frac{\partial}{\partial r^*}(r^*v^*k^*)\\&\quad=\frac{\partial}{\partial x^*}\left\{\frac{1}{Re}\left(1+\frac{Re_t}{\sigma_k}\right)\frac{\partial k^*}{\partial x^*}\right\}\\&\qquad+\frac{1}{r^*}\frac{\partial}{\partial r^*}\left\{r^*\frac{1}{Re}\left(1+\frac{Re_t}{\sigma_k}\right)\frac{\partial k^*}{\partial r^*}\right\}\\&\qquad+\frac{Re_t}{Re}\left(\frac{\partial u^*}{\partial r^*}\right)^2-(\tilde{\varepsilon}^*+D)-\frac{2}{Re}\left(\frac{\partial\sqrt{k^*}}{\partial r^*}\right)^2\end{aligned}\tag{12}$$

$$\begin{aligned}&\frac{\partial}{\partial x^*}(u^*\varepsilon^*)+\frac{1}{r^*}\frac{\partial}{\partial r^*}(r^*v^*\varepsilon^*)\\&\quad=\frac{\partial}{\partial x^*}\left\{\frac{1}{Re}\left(1+\frac{Re_t}{\sigma_\varepsilon}\right)\frac{\partial \varepsilon^*}{\partial x^*}\right\}\\&\qquad+\frac{1}{r^*}\frac{\partial}{\partial r^*}\left\{r^*\frac{1}{Re}\left(1+\frac{Re_t}{\sigma_\varepsilon}\right)\frac{\partial \varepsilon^*}{\partial r^*}\right\}\\&\qquad+\frac{Re_t}{Re}C_1f_1\frac{\varepsilon^*}{{}^*k}\left(\frac{\partial u^*}{\partial r^*}\right)^2-C_2f_2\frac{(\varepsilon^*)^2}{k^*}\\&\qquad+\frac{2}{Re^2}(1+Re_t)\left(\frac{\partial^2u^*}{\partial r^{*2}}\right)^2\end{aligned}\tag{13}$$

The model equations for turbulent parameters, i.e., k and ε equations are non-dimensionalized using the following non-dimensional parameters:

$$k^*=\frac{k}{U^2}\quad\text{and}\quad\varepsilon^*=\frac{\varepsilon}{(U^3/R_r)}\tag{14}$$

Here turbulent kinematic viscosity is given by

$$v_t=C_\mu f_\mu\frac{k^2}{\varepsilon}\tag{15}$$

Wall damping functions are given by

$$\begin{aligned}&f_1=1.0\\&f_2=1.0-0.3\exp(-Re_t^2)\\&f_\mu=\exp\left[\frac{-3.4}{1+\left(\frac{Re_t}{50}\right)^2}\right]\end{aligned}\tag{16}$$

where turbulent Reynolds number

$$Re_t=\frac{k^2}{v\tilde{\varepsilon}}\tag{17}$$

The model constants are

$$\begin{aligned}&C_\mu=0.09,\quad C_1=1.44,\quad C_2=1.92,\\&\sigma_k=1.0,\quad\sigma_\varepsilon=1.3\end{aligned}\tag{18}$$

3.2. Resistances to airflow

Various solid obstacles present in the tower like packing material, etc. and the liquid flow offer resistances to the flow of air in both axial and radial directions. It is highly difficult to define each solid object as an interior boundary. Therefore these are accounted for by including the resistances offered by these obstacles and liquor flow in the momentum equations. These are expressed in integral form for each control cell [2] as

$$\int f_x\,\mathrm{d}V=N\frac{1}{2}\rho u^2\Delta V+N_l\frac{1}{2}\rho u^2\Delta A+N_e\frac{1}{2}\rho u^2\Delta A\tag{19}$$

$$\int f_r\,\mathrm{d}V=N\frac{1}{2}\rho v^2\Delta V+N_l\frac{1}{2}\rho v^2\Delta A+N_e\frac{1}{2}\rho v^2\Delta A\tag{20}$$

where ΔV is the volume, and ΔA is the area of the control cell face normal to the velocity component. N is the number of velocity heads lost per unit air travel distance. N_l and N_e are the total number of velocity heads lost in louvers and eliminator respectively.

3.3. Heat and mass transfer

From Reynolds flux model of interface heat and mass transfer, together with conservation equations for liquor, air and moisture fraction

$$\frac{df_a}{f_i-f_a}(1-f_i)=\frac{L}{G}\frac{dh_l}{(h_i-h_a)}\tag{21}$$

Eq. (21) can be treated as a finite difference equation and for finite increments in h_l, dh_l, the increments in f_a, df_a, may be evaluated with known values of f_i, h_i, h_a, L and G. Once moisture fraction at outlet is known, mass transfer rate can be calculated as

$$m'''=G(W_{ao}-W_{ai})\rho_a\tag{22}$$

Then, the empirical mass transfer coefficient K and heat transfer rate are calculated from the following equations:

$$m'''=Ka(f_i-f_a)\tag{23}$$

$$q'''=Ka(h_i-h_a)\tag{24}$$

3.4. Properties of moist air and liquor

Properties of moist air like moisture fraction, specific humidity, enthalpy, etc. are calculated by equations for psychrometric properties [14]. These equations are derived from fundamental equations for ideal gas mixtures. Effect of ambient pressure is also included in these equations. Hence, these equations give more accurate results and increase the range of applicability of method than the polynomial curve fitted equations or tables.

Major constituent of soak liquor is sodium chloride salt. Since more than 80% of the salt in seawater is also sodium chloride, seawater properties are used for the thermo-physical properties of soak liquor [13].

3.5. Boundary conditions

As the problem is elliptic in space, boundary conditions for all dependent variables must be specified on all confining surfaces. In addition, the following quantities are specified as system boundary conditions: liquor flow rate, either temperature range of liquor or liquor temperature at inlet, dry bulb temperature, either wet bulb temperature or relative humidity and ambient pressure.

3.6. Method of solution

A modified version of MAC (Marker and Cell) method [1,6,8] is used to obtain the numerical solution of governing equations. Computational domain is divided into a number of control cells. Staggered grid arrangements are used in which velocity components are defined at the mid-point of cell faces to which they are normal. Pressure is defined at the center of cell. Computational domain and grid are shown in Fig. 2. In order to define boundary conditions in a staggered grid arrangement, it is necessary to consider the imaginary cells surrounding the physical domain as shown in Fig. 3. Boundary conditions are imposed by setting appropriate velocities in the imaginary cells. At walls, no-slip condition is employed. For this the normal velocity is set to zero and the tangential velocity components should also be zero. At the axis axisymmetric boundary condition is employed. For this, the normal velocity should be zero and the tangential velocities should have no normal gradient. At the inlet, a uniform profile is given to normal velocity and other component is set to zero. At the outlet, outflow boundary conditions is employed, i.e., second derivatives of the dependent variables in flow direction are set to zero to ensure smooth transition through the outflow boundary. Time dependent equations in non-dimensional form are discretized with finite difference schemes.

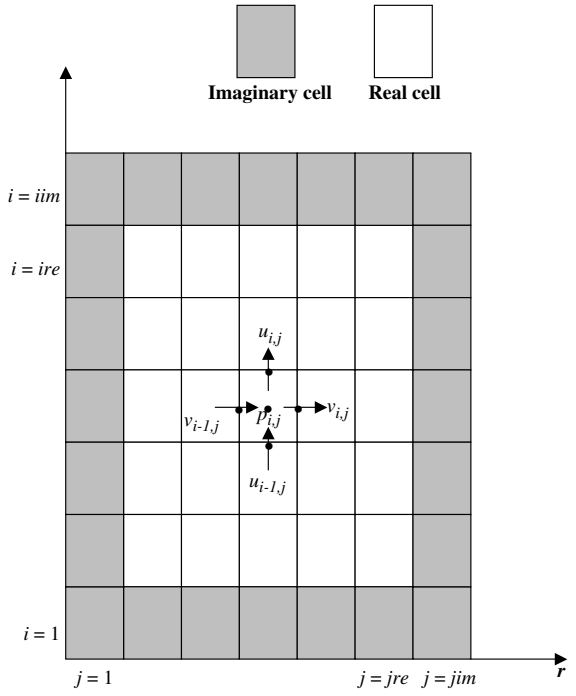

Fig. 3. Staggered grid.

All the terms in the governing equations are discretized with finite difference schemes. Convective terms are discretized using first and third order upwind schemes [10]. Third order upwind scheme is employed for interior points and first order upwind scheme is employed for the points near boundary.

A numerical solution is achieved by marching in time direction. A second-order Adam–Bashforth scheme is utilized for time marching. The solution is obtained in two steps. Initially an explicit calculation is performed which uses previous time velocities and pressures to determine the provisional velocities through the accelerations caused by convection, viscous stresses and pressure gradients. In order to ensure mass conservation in all cells, an iterative algorithm is employed in the second step, which adjusts the velocities through changes in the pressure field. These iterations continue until divergence free velocity field is obtained. However, for this purpose the divergence in each cell is towed below a pre-assigned small quantity. In the present computation this quantity is taken as 10^{-4}. As the problem is steady in physical sense, after some finite steps in time direction, two consecutive steps will show identical results. Then, steady state solution is considered achieved. Then, energy and moisture fraction equations of air and continuity and energy equations of liquor are solved.

The conditions necessary to prevent numerical instabilities are determined from the Courant–Friedrichs–Lewy (CFL) condition and grid Fourier numbers that require

$$\delta t < \min\left\{\frac{\delta x}{|u|}, \frac{\delta r}{|v|}\right\} \tag{25}$$

$$\delta t < \frac{1}{2}\left\{\frac{(\delta x^2 \delta r^2)}{\delta x^2 + \delta r^2}\right\} \tag{26}$$

Performance parameters are calculated as follows:

Convective mass transfer coefficient is calculated as

$$h_{\mathrm{M}} = \frac{K}{\rho_{\mathrm{m}}} \tag{27}$$

Sherwood number is determined from the following equation:

$$Sh = \frac{h_{\mathrm{M}} L_{\mathrm{c}}}{D_v} \tag{28}$$

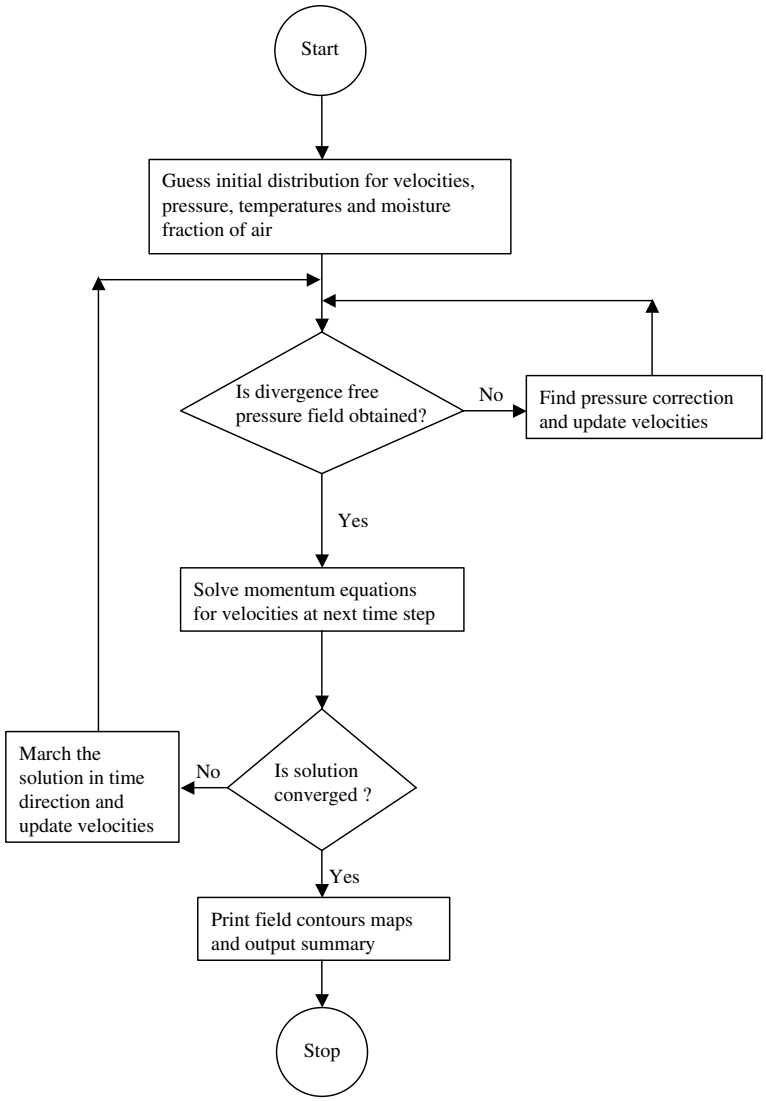

Fig. 4. Main steps in the solution methodology.

where D_v = diffusion coefficient ($mm^2\ s^{-1}$) and is given by

$$D_v = \frac{0.926}{p}\left(\frac{T_a^{2.5}}{T_a + 245}\right) \tag{29}$$

The model has been embodied (Fig. 4) into a computer code using 'C' language. This model can be used for mechanical draft systems of both circular and rectangular cross sections. Setting r to unity and $\partial/\partial r$ to $\partial/\partial y$, governing equations become appropriate for Cartesian coordinates. The model can be used for designing a new system. For a given set of operating conditions, it gives the tower dimensions required for evaporation during a specified time. The model can be used for optimizing the existing systems. For a given set of ambient conditions, tower details and volume of liquid to be evaporated, it gives the optimal values of flow rates of air & liquid and inlet temperature of liquid for enhanced evaporation rate.

4. Experimentation

A forced convective evaporation system on laboratory scale has been constructed for carrying out experimentation as shown in Fig. 1 [7]. Immersions heaters are used as heat source. Flow rate of liquor is controlled by ball valves and it is measured with a calibrated flow meter. Evaporation rate is measured with the volume of make up water added from the tank. Typical calibrated instruments used for measure-

Table 1
Instruments and their details

S. no.	Parameter	Instrument	Unit of measurement	Accuracy	Range	Error in measurement (%)
1	Dry bulb temperature and liquor temperature	Copper constantan thermocouple (T type) with data acquisition system	°C	0.1 °C	0–70 °C	±0.4
2	Volume flow rate of liquor	Flow meter with stop watch	$m^3 h^{-1}$	0.001 $m^3 h^{-1}$	0–20 $m^3 h^{-1}$	±0.0102
3	Air velocity	Vane type anemometer	$m s^{-1}$	0.1 $m s^{-1}$	0–10 $m s^{-1}$	±0.5
4	Relative humidity	RH meter	%	0.1%	20–100%	±0.2587
5	Air pressure drop	U-tube manometer	mm of water	1 mm	0–200 mm	±0.1
6	Evaporation rate	Piezometer and stop watch	$m^3 h^{-1}$	1 mm, 0.01 s	0–500 mm, 0–99.99 min	±2.0025

ments, units of measurement, their accuracy and the error involved in measured and derived quantities (evaluated by error analysis) are shown in Table 1. Experiments were initially conducted with pure water. Measurement of all necessary parameters was made at different flow rates and temperatures of water. To study the influence of the system performance at varying atmospheric conditions, experiments were repeated at different times in a day, on different days and different seasons. Later experiments were carried out in a similar way with clarified soak liquor at different concentrations and necessary data were collected. The concentration was limited to 12.5% as fluid flow problems experienced at that state.

5. Results and discussion

Predicted thermal performances compare well with the available data in literature. The distributions of air velocities, pressure, moisture fraction, temperature, and liquor temperatures have been assessed from the considerations of physical plausibility only, since no experimental data are available for comparison.

Detailed experimental measurement of flow distributions in the cooling tower for model validation is not available due to the complexity of internal flow measurements. Hence, validation of the present model was restricted to the existing outlet thermal performances. Table 2 provides the comparison between present

Table 2
Comparison of performance between present model, field test data and VERA2D for a mechanical draft cooling tower

Test no.	Specified conditions					Approach (°C)				
	Range (°C)	DBT (°C)	WBT (°C)	Water flow rate ($kg s^{-1}$)	Air flow rate ($kg s^{-1}$)	Measured	Predicted by present model	Predicted by VERA2D	Difference between predicted and measured values	
									Present	VERA2D
1	8.33	29.00	21.38	1118.25	647.2	9.16	9.175	9.279	−0.015	−0.119
2	8.29	29.80	21.87	1148.57	644.5	8.94	8.966	9.301	−0.026	−0.361
3	8.10	30.25	22.25	1153.68	643.8	8.85	8.678	9.045	0.172	−0.195
4	8.11	30.30	22.28	1148.96	644.0	8.76	8.665	9.003	0.095	−0.243
5	8.06	30.50	22.39	1152.51	643.7	8.64	8.588	8.950	0.052	−0.310
6	7.78	32.00	23.85	1143.45	642.3	7.34	7.775	8.108	−0.435	−0.768
7	7.73	30.25	22.26	1132.82	645.5	8.48	8.392	8.594	0.088	−0.114
8	7.56	31.00	22.67	1130.46	644.9	8.16	8.098	8.289	0.062	−0.129
9	7.31	31.80	23.56	1126.52	644.1	7.54	7.559	7.740	−0.019	−0.200
10	8.02	30.15	22.16	1155.66	644.0	8.70	8.665	9.035	0.035	−0.335
11	8.20	29.55	21.75	1153.29	644.6	8.96	8.966	9.318	−0.006	−0.358
12	8.09	29.45	21.66	1137.94	645.8	8.97	8.909	9.146	0.061	−0.176
13	8.15	28.85	21.66	1137.94	646.5	9.14	8.952	9.352	0.188	−0.212
14	7.79	30.00	22.02	1137.94	645.5	8.65	8.543	8.773	0.107	−0.123
15	8.11	28.95	21.31	1137.94	646.4	8.95	9.078	9.301	−0.128	−0.361

Table 3
Comparison between theoretical and experimental performance of forced convective evaporation system

S. no.	Operating conditions						Evaporation rate ($m^3 h^{-1}$)			Sherwood number		
	Range (°C)	DBT (°C)	RH (%)	Water flow rate ($kg s^{-1}$)	Air flow rate ($kg s^{-1}$)	Salt concentration (%)	Actual	Predicted	% error	Actual	Predicted	% error
1	1.5	32.525	62.1	3.295	0.893	0.0	0.0292	0.02668	8.63	495.394	469.66	5.19
2	2.9	32.15	48.9	2.745	1.2	0.0	0.0401	0.04423	−10.3	819.707	808.56	1.36
3	2.3	31.2	65	3.164	1.251	2.467	0.0347	0.03786	−8.35	996.512	1054.95	−5.86
4	2.5	29.167	67.7	3.229	1.2	2.467	0.0362	0.03828	−5.75	871.36	834.41	4.24
5	2.4	37.15	48.4	2.2212	1.06	6.014	0.0334	0.02868	14.13	332.921	356.98	−7.22
6	3.1	29.763	58.9	2.6022	1.088	6.014	0.0378	0.03933	−4.05	847.265	884.44	−4.39
7	1.6	31.0	72.1	2.7698	1.228	12.52	0.0254	0.02336	8.03	604.78	637.044	−5.33
8	2.6	34.225	63.8	2.7319	1.291	12.52	0.0331	0.03436	−3.81	561.54	595.115	−5.98

model's prediction of thermal performance with existing field test data and predictions obtained by VERA2D of Majumdar et al. [3]. It can be observed from the comparison that the present model gives better predictions than VERA2D. This can be attributed to the fact that VERA2D employed a length scale turbulence model, which solves one equation for turbulent viscosity. The present model employs k–ε turbulence model, which solves two equations for turbulent viscosity. Present model calculates mass transfer from an equation derived from fundamentals thereby eliminating the need of using the empirical coefficients for mass transfer coefficient followed by other models.

For the computation, a typical non-uniform grid of size 112×114 is used. There are 10 cells of value 0.0008, 46 cells of value 0.00158 and 58 cells of value 0.0158 in

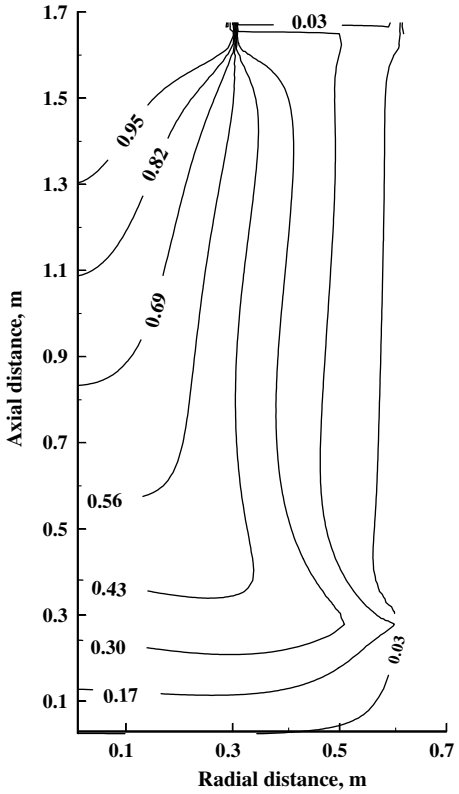

Fig. 5. Predicted contours of u velocity.

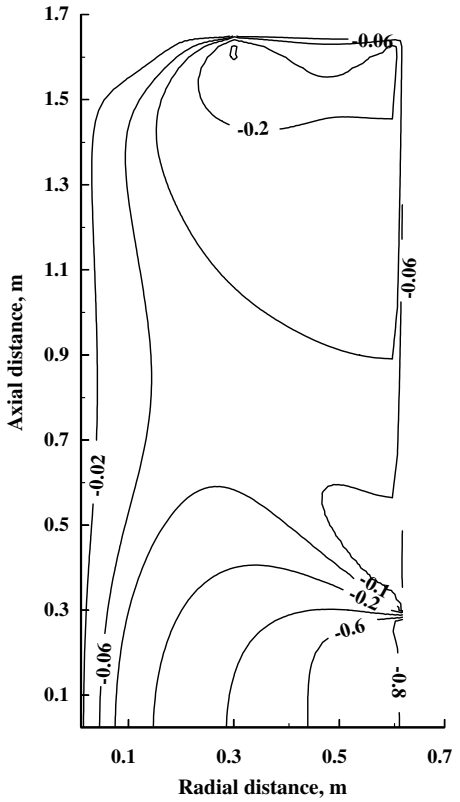

Fig. 6. Predicted contours of v velocity.

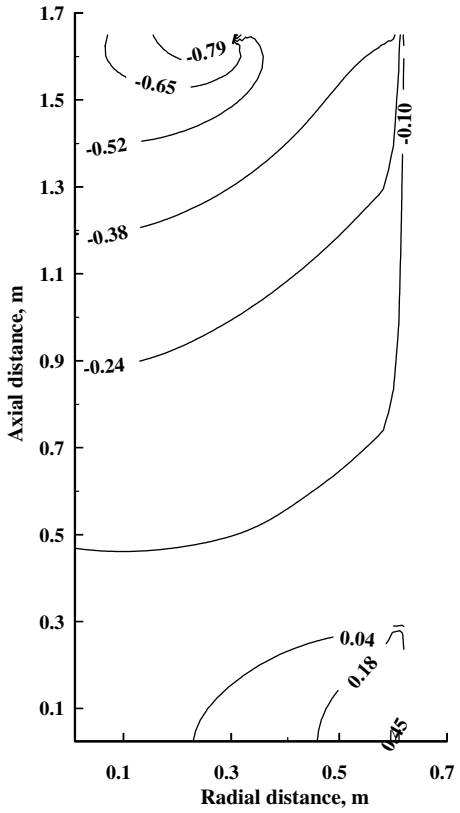

Fig. 7. Predicted contours of static pressure.

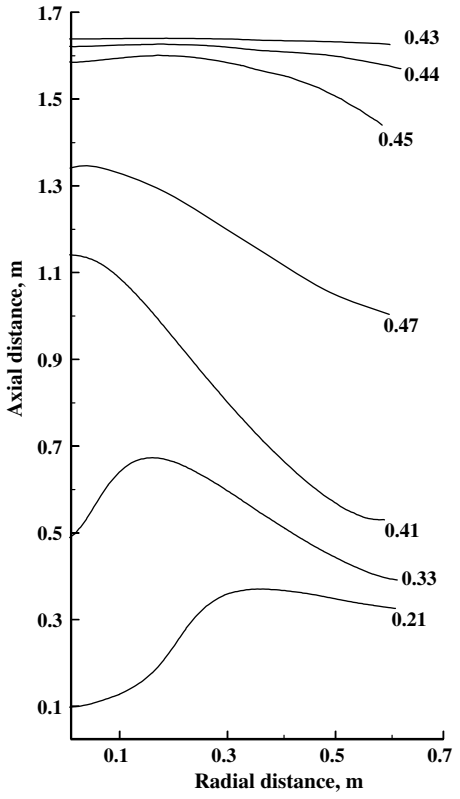

Fig. 8. Predicted contours of dry bulb temperature of air.

radial direction (r^*). There are 20 cells of value 0.008 and 92 cells of value 0.0285 in axial direction (x^*). The mesh has been refined at the walls to capture the steep gradients of turbulent parameters. Several meshes of different sizes have been used and the mesh of size 112×114 is found to give grid independent results. Refining the mesh further did not produce any appreciable change in results. Initial values for all the dependent variables are assumed. For velocity, axial component is taken as unity while radial component is assumed to be zero. Free stream conditions are assumed for other parameters. For the grid mentioned above, the code is found to converge in 9024 iterations in time direction. The CPU time taken for convergence is 631.68 s. The machine used for computation is a Pentium IV with processor speed of 1.7 GHz and a RAM of 512 MB. Theoretical performance is compared with the results evaluated by conducting experiments on forced convective evaporation system at Chennai, India (Latitude = 13°N) using soak liquor. Predicted results agree well with the experimental results as shown in Table 3. Computations have been carried out at the following operating conditions:

Mass flow rate of soak liquor	4 $kg\,s^{-1}$
Mass flow rate of air	3 $kg\,s^{-1}$
Temperature range of liquor	5 °C
Soak liquor temperature at inlet	35 °C
Dry bulb temperature of air	35 °C
Relative humidity of air at inlet	50%
Ambient pressure	1.01325 bar

Figs. 5 and 6 show the contours of non-dimensional u-velocity (axial) and v-velocity (radial) respectively. As air enters the system radially at the bottom, magnitude of u-velocity is less and v-velocity is more near the inlet. As the flow progresses towards the outlet, magnitude of u-velocity increases and v-velocity decreases. Because of the axial outlet, u-velocity is more near the outlet. Velocity is minimum at wall because of the no slip condition.

Fig. 7 presents the distribution of static pressure in the system. Because of the induced draft fan, pressure inside is less than that of the ambient, being minimum near outlet. This pressure gradient enables air to flow from inlet to outlet.

Fig. 8 discerns the contours of non-dimensional dry bulb temperature of air in the system. As the flow

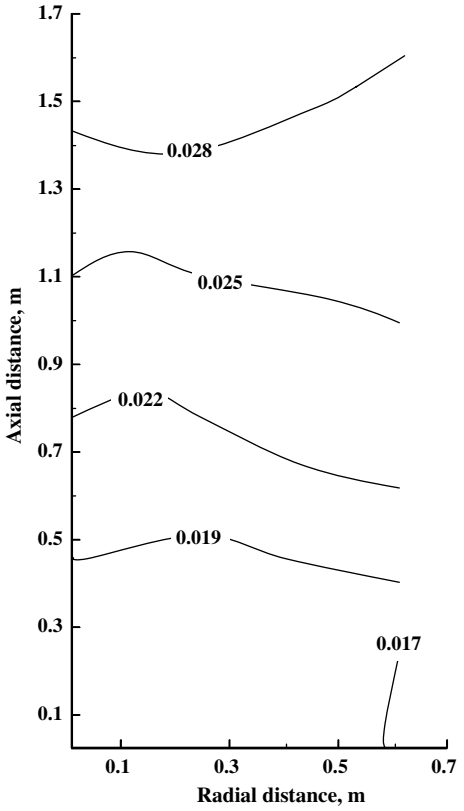

Fig. 9. Predicted contours of mass fraction of moisture in air.

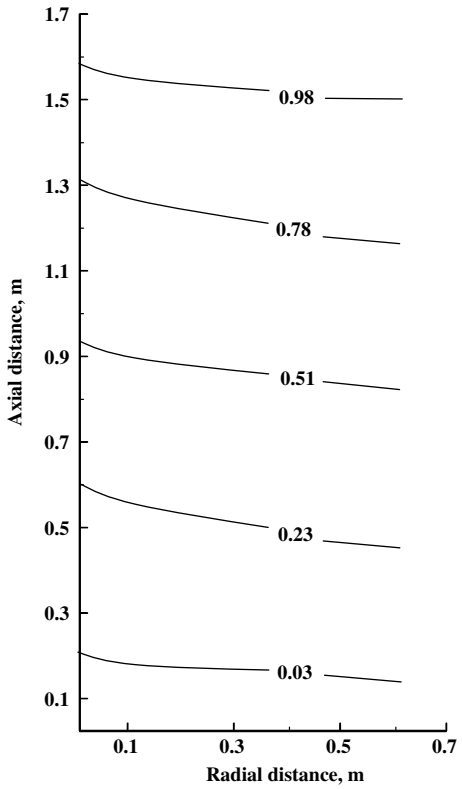

Fig. 10. Predicted contours of liquor temperature.

progresses from inlet, temperature decreases because of the lower local liquor temperature. After that it increases because of the higher liquor temperature.

Fig. 9 depicts the distribution of mass fraction of moisture in air. As is evident, it increases from inlet to exit because of the mass transfer from liquor to air.

Fig. 10 shows the contours of non-dimensional liquor temperature. Even though liquor flow is considered to be one-dimensional, contours show considerable variation. This is because of the non-uniformity of airflow in the tower.

Fig. 11 discerns the effect of mass flow rate of liquor on Sherwood number at different salt concentrations. As the mass flow rate increases, the contact surface area between liquor and air increases. This increases the mass transfer coefficient resulting in increased Sherwood number. As the concentration increases, the partial pressure difference between interface and air decreases. Being a measure of non-dimensional concentration gradient, Sherwood number decreases with increase in salt concentration.

Fig. 12 depicts the effect of dry bulb temperature of air on Sherwood number. Increase in dry bulb temperature increases the partial pressure of water vapour thereby reducing the partial pressure difference between

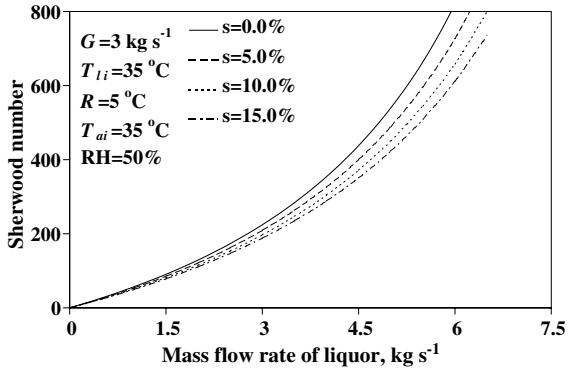

Fig. 11. Effect of mass flow rate of liquor on Sherwood number.

interface and air. It also decreases the diffusion coefficient resulting in reduced Sherwood number.

The effect of temperature range of soak liquor on Sherwood number is shown in Fig. 13. As the range increases, mean temperature of liquor and hence the partial pressure of vapour at the interface increases resulting in higher mass transfer. Therefore, Sher-

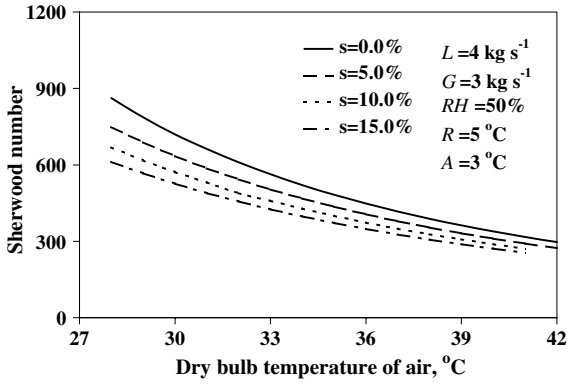

Fig. 12. Effect of dry bulb temperature on Sherwood number.

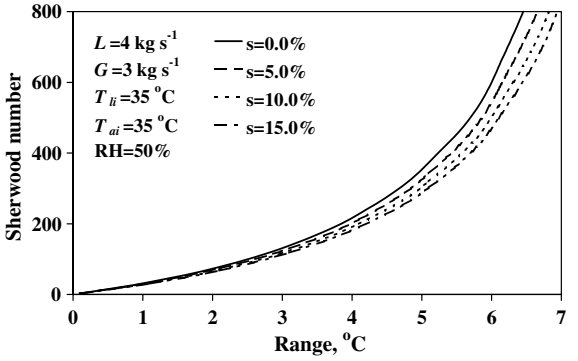

Fig. 13. Effect of temperature range of liquor on Sherwood number.

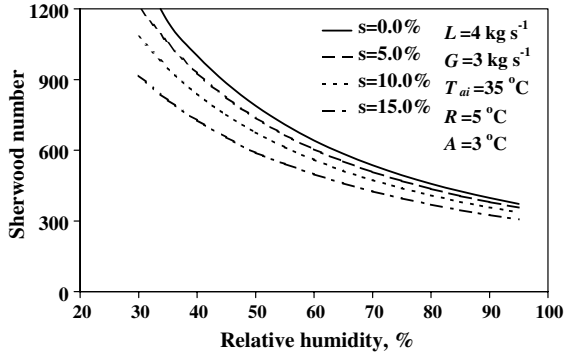

Fig. 14. Effect of relative humidity on Sherwood number.

wood number increases with temperature range of liquor.

Fig. 14 presents the effect of relative humidity on Sherwood number. As the relative humidity increases, the partial pressure of air increases decreasing the driving potential of partial pressure difference. This results in reduced Sherwood number. As explained earlier, Sherwood number decreases with increase in concentration.

6. Conclusions

In this paper, a numerical technique has been presented to simulate the performance of forced convective evaporation system. A general mathematical model applicable for mechanical draft towers of counter flow or cross flow has been described. The model is applicable for geometries of circular as well as rectangular cross section. The model has been embodied into a computer code, which can be used for performance evaluation as well as for design optimization studies. Predicted results agree well with the available data in the literature and give closer results than VERA2D model. Presented results demonstrate the accuracy and stability of the model. The predicted global and local quantities are self-consistent and physically plausible.

References

[1] A.J. Chorin, A numerical method for solving incompressible viscous flow problems, J. Comput. Phys. 2 (1967) 12–26.
[2] A.K. Majumdar, A.K. Singhal, D.B. Spalding, Numerical modeling of wet cooling towers—Part 1: Mathematical and physical models, Trans. ASME, J. Heat Transfer 105 (1983) 728–735.
[3] A.K. Majumdar, A.K. Singhal, D.B. Spalding, Numerical modeling of wet cooling towers—Part 2: Application to natural and mechanical draft towers, Trans. ASME, J. Heat Transfer 105 (1983) 736–743.
[4] D.R. Baker, H.A. Shryok, A comprehensive approach to the analysis of cooling tower performance, ASME J. Heat Transfer 83 (1961) 339–349.
[5] F. Merkel, Evaporative cooling, Zeits. Verein Deutsc. Ingeni. 70 (1926) 123–128.
[6] H.H. Francis, J.E. Welch, Numerical calculation of time-dependent viscous incompressible flow of fluid with free surface, Phys. Fluids 8 (1965) 2182–2189.
[7] G.V.S. Sesha Girish, A. Mani, Experimental studies on forced convective evaporation system for tannery effluent (Soak liquor), Environ. Prog., submitted for publication.
[8] J.A. Viecelli, A computing method for incompressible flows bounded by moving walls, J. Comput. Phys. 8 (1971) 119–143.
[9] J.W. Sutherland, Analysis of mechanical-draught counter-flow air/water cooling towers, Trans. ASME, J. Heat Transfer 105 (1983) 576–583.
[10] S. Shirayama, Construction of modified third-order upwind schemes for stretched meshes, AIAA J. 30 (5) (1992) 1237–1242.
[11] T.J. Marseille, J.S. Schliesing, D.M. Bell, B.M. Johnson, Extending cooling tower thermal performance prediction

using a liquid-side film resistance model, Heat Transfer Eng. 12 (1991) 19–30.
[12] W.P. Jones, B.E. Launder, The prediction of laminarization with a two equation model of turbulence, Int. J. Heat Mass Transfer 15 (1972) 301–314.
[13] A.H. Khan, Desalination Processes and Multistage Flash Distillation Practice, Elsevier, Amsterdam, 1986.
[14] ASHRAE Handbook: Fundamentals (SI), 1997 (Chapters 5&6).